

Effect of electromagnetic boundary conditions on convective dynamo onset

M. Fontana,* P. D. Mininni, and P. Dmitruk

*Universidad de Buenos Aires, Facultad de Ciencias Exactas y Naturales,
Departamento de Física, Ciudad Universitaria, 1428 Buenos Aires, Argentina, and
CONICET - Universidad de Buenos Aires, Instituto de Física del Plasma (INFIP),
Ciudad Universitaria, 1428 Buenos Aires, Argentina.*

We present a high-order numerical study of the dependence of the dynamo onset on different electromagnetic boundary conditions, in convecting Boussinesq flows forced by a temperature gradient. Perfectly conducting boundaries, vacuum, and mixed electromagnetic boundary conditions are considered, using a method that treats fields and boundary conditions with close to spectral accuracy. Having one or two conducting boundaries greatly facilitates dynamo action. For the mixed case it is shown that the critical magnetic Reynolds number becomes independent of the Rayleigh number, Ra , for sufficiently large Ra .

I. INTRODUCTION

Magnetic fields are ubiquitous in nature, defining the dynamics of a multitude of physical systems from the atomic scale up to galactic evolution. Of particular interest is the mechanism by which magnetic fields are amplified inside celestial objects, such as the Earth or the Sun, to name two familiar examples of this phenomenon. The commonly accepted explanation for said origin is the transformation of kinetic energy into magnetic energy taking place in an electrically conducting fluid layer inside the celestial object, i.e., a magnetohydrodynamic (MHD) dynamo [1–5]. In the case of the Earth, for instance, that layer is the fluid outer core, and the forcing mechanism that drives the flow is thought to be the thermochemical convection due to the cooling of the Earth’s interior [6, 7].

Although the MHD dynamo mechanism was first proposed at the beginning of the 20th century, it was quickly realized that simple symmetric non-turbulent flows were unable to sustain the magnetic fields commonly observed in nature [8, 9]. However, the requirement for the flow to be turbulent notably increases the experimental and numerical difficulties of reproducing celestial dynamo generation [10–14]. Indeed, it was just in the last couple of decades that both laboratory experiments and numerical simulations were able to attain dynamo regimes which exhibit the kind of features found in celestial magnetic fields, such as a high degree of symmetry, polarity inversions, or periodic modulations [15–17]. In fact, the task of experimentally obtaining a self-sustaining dynamo regime from flow conditions which more closely resemble those found in celestial bodies is still being actively pursued [18–21].

Electromagnetic boundary conditions are known to have an impact on the feasibility of attaining a self-sustaining dynamo at a given power input, together with domain geometry, the forcing mechanism, and the fluid transport coefficients [22–25]. However, numerically studying different boundary conditions on equal footing, and with the same numerical convergence, provides a challenge. Perhaps the best confirmation of the influence of electromagnetic boundary conditions on dynamo feasibility is given by the VKS experiment [17]. In this experiment using liquid sodium, it was shown that changing propellers from stainless steel to ferromagnetic composition resulted in measurable differences on the power input required to attain magnetic amplification.

In this letter we present a detailed numerical study of the influence of electromagnetic boundary conditions in the minimum magnetic Reynolds number required to observe dynamo action on a convecting flow forced by a temperature gradient. To this purpose direct numerical simulations (DNSs) of the three-dimensional (3D) non-linear MHD equations are employed, using a numerical method which guarantees quasi-spectral convergence for several types of boundary conditions while enforcing a solenoidal magnetic field to machine precision in non-trivial geometries [26, 27]. In particular, perfectly conducting or vacuum electromagnetic conditions are considered at the boundaries, together with a combination of both scenarios. We then pick the latter boundary condition because of its relevance for planetary dynamos, and study how increasing the strength of convection affects the requirements to reach the dynamo onset.

* mfontana@df.uba.ar

II. GOVERNING EQUATIONS

We consider a magnetofluid in a rectangular domain Γ whose dimensions are $L_x \times L_y \times L_z = (2\pi \times 2\pi \times 1)L_0$, where L_0 is a unitary length. This domain is periodic in the \hat{x} and \hat{y} directions and has impermeable isothermic walls which cannot slip at $z/L_0 = 0$ and 1. Gravity points in the $-\hat{z}$ direction. The dynamics is described under the Boussinesq approximation by the incompressible MHD equations,

$$\frac{\partial \mathbf{u}}{\partial t} + (\mathbf{u} \cdot \nabla) \mathbf{u} = -\nabla p + \gamma \theta \hat{z} + (\nabla \times \mathbf{b}) \times \mathbf{b} + \nu \nabla^2 \mathbf{u}, \quad \nabla \cdot \mathbf{u} = 0, \quad (1)$$

$$\frac{\partial \mathbf{b}}{\partial t} = \nabla \times (\mathbf{u} \times \mathbf{b}) + \eta \nabla^2 \mathbf{b}, \quad \nabla \cdot \mathbf{b} = 0, \quad (2)$$

$$\frac{\partial \theta}{\partial t} + (\mathbf{u} \cdot \nabla) \theta = \gamma u_z + \kappa \nabla^2 \theta, \quad (3)$$

with the mechanical and thermal boundary conditions $\mathbf{u} = \mathbf{0}$ and $\theta = 0$ at $z/L_0 = 0$ and 1. Here, \mathbf{u} , \mathbf{b} , and θ are the velocity, magnetic, and temperature fluctuation fields respectively, whereas ν , η , and κ are the momentum, magnetic, and temperature diffusivities. The parameter γ controls the intensity of the buoyancy term, which relates to the temperature difference between the plates ΔT as $\gamma = \sqrt{\alpha \Delta T g / L_z}$, with α the thermal expansion coefficient and g the acceleration of gravity. The temperature fluctuation is obtained as the difference between the total temperature of the fluid, T , and a linear profile corresponding to the purely conductive solution, T_0 , as $T' = T - T_0$, which is then expressed in velocity units as $\theta = \gamma L_z T' / \Delta T$ [26]. Similarly, the magnetic field \mathbf{b} is also expressed in velocity units as $\mathbf{b} = \mathbf{B} / \sqrt{\mu \rho}$, with \mathbf{B} the magnetic field in SI units, μ the magnetic permeability, and ρ the mean fluid density.

There are several ways to obtain dimensionless versions of Eqs. (1) to (3). A usual set of parameters to describe the incompressible Boussinesq MHD equations is given by the kinematic Reynolds number Re , the magnetic Reynolds number Rm , the Rayleigh number Ra , and the thermal and magnetic Prandtl numbers, Pr and Pm respectively [26, 28, 29]. They can be expressed in terms of dimensional quantities as

$$Re = \frac{UL}{\nu}, \quad Rm = \frac{UL}{\eta}, \quad Ra = \frac{\gamma^2 L^4}{\nu \kappa}, \quad Pr = \frac{\kappa}{\nu}, \quad Pm = \frac{\eta}{\nu}, \quad (4)$$

with U and L a characteristic speed and lengthscale of the flow. In this work we consider U to be the r.m.s. value of the flow speed, and $L = L_z/2$. Physically, Re is the ratio between momentum advection and momentum diffusion. Similarly, Rm measures the ratio of magnetic induction to Ohmic dissipation. Ra is the ratio of the thermal diffusion time to the characteristic time of a fluid element freely ascending due to buoyancy. Finally, Pr and Pm compare the time scale of momentum diffusion against the diffusive time scales of the temperature and magnetic fields, respectively.

As previously mentioned, in this work we consider three distinct scenarios for the electromagnetic boundary conditions: perfectly conducting walls at $z/L = 0$ and 1, vacuum surroundings, and their combination. All these boundary conditions are of interest for different situations in geodynamos and stellar dynamos, as well as for laboratory dynamo experiments [16, 17, 30]. In the first case, perfectly conducting walls are thought to approximate the boundary of the inner to outer Earth core [31]. In that case there can be no magnetic flux nor tangential electric field at the walls [32]. This can be attained by enforcing the following pair of relations at either $z/L_0 = 0$ or 1 (or at both boundaries):

$$\mathbf{j} \times \hat{z} = \mathbf{0}, \quad \partial_t \mathbf{b} \cdot \hat{z} = 0, \quad (5)$$

where $\mathbf{j} = \nabla \times \mathbf{b}$ is the current density, which at the boundary is proportional to the electric field \mathbf{E} if the walls are stationary. The situation of vacuum surroundings approximates the physical scenario found in stars, and resembles the insulating properties of the Earth interior in the boundary between the outer core and the mantle [6]. If the electrical permittivity of the fluid is assumed to be close to that of vacuum, the vacuum surroundings scenario requires the continuity of the magnetic field at the wall, as do insulating boundary conditions, together with the continuity of the normal component of the electric field [32]. More precisely, the conditions

$$[\mathbf{b}] = \mathbf{0}, \quad [E_z] = 0, \quad (6)$$

must be obeyed at $z/L_0 = 0$ or $z = 1$ (or at both places). Here $[\cdot]$ denotes the jump condition at the boundary. Note that as vacuum surrounds the magnetofluid, the magnetic field in the exterior of the box must be compatible with a scalar potential representation, as a result of the absence of currents there. Equation (6) requires the enforcement of that compatibility relation for \mathbf{b} at the walls. Finally, the mixed or combined case corresponds to imposing one boundary condition (e.g., perfect conductor) at $z/L_0 = 0$, and the other boundary condition (e.g., vacuum surroundings) at $z/L_0 = 1$. Besides its relevance for the geodynamo, there are experiments which seek to obtain self-sustaining dynamos employing similar conditions [19, 20], although that goal has so far been elusive.

TABLE I. Simulations with $256 \times 256 \times 103$ grid points and three different boundary conditions. Run is the label for each simulation, with C, M and V denoting conducting, mixed, and vacuum boundary conditions. Re and Rm are the kinetic and magnetic Reynolds number respectively, and Pm is the magnetic Prandtl number. σ is the growing rate of the magnetic energy, with negative values corresponding to decaying solutions. All simulations have $Ra = 2.25 \times 10^6$, $Re = 6.06 \times 10^2$, and $Pr = 1$.

Run	Rm	Pm	σ	Run	Rm	Pm	σ
C1	2.43×10^2	4.00×10^{-1}	0.41	M1	1.21×10^2	2.00×10^{-1}	0.13
C2	1.21×10^2	2.00×10^{-1}	0.32	M2	6.06×10^1	1.00×10^{-1}	0.07
C3	6.06×10^1	1.00×10^{-1}	0.26	M3	2.42×10^1	4.00×10^{-2}	-0.01
C4	2.41×10^1	4.00×10^{-2}	0.19	M4	1.21×10^1	2.00×10^{-2}	-0.07
C5	1.20×10^1	2.00×10^{-2}	0.11				
C6	6.06	1.00×10^{-2}	0.05	V1	6.06×10^2	1.00	0.40
C7	2.40	4.00×10^{-3}	0.03	V2	4.83×10^2	8.00×10^{-1}	0.25
C8	1.20	2.00×10^{-3}	0.00	V3	3.03×10^2	5.00×10^{-1}	0.01
C9	8.64×10^{-1}	1.43×10^{-3}	-0.08	V4	2.41×10^2	4.00×10^{-1}	-0.07
C10	6.06×10^{-1}	1.00×10^{-3}	-0.32	V5	1.21×10^2	2.00×10^{-1}	-0.18

A self-sustaining dynamo must be able to amplify a seed magnetic field, increasing the initial magnetic energy of the system E^b as long as the flow is maintained or until non-linear saturation is reached. For systems operating at finite magnetic Reynolds number, this implies that magnetic induction, given by the term $\nabla \times (\mathbf{u} \times \mathbf{b})$, must overcome the Ohmmic losses associated with the term $\eta \nabla^2 \mathbf{b}$. To study the feasibility of obtaining a self-sustaining dynamo for a given value of Rm and a certain geometry, it is common practice to consider the flow to be known and an initial magnetic energy to be much smaller than the kinetic one, E^u , leading to the kinematic dynamo problem. A common strategy to study the kinematic dynamo problem theoretically is to neglect the effect of the magnetic field on the flow evolution (that is, the Lorentz force), and thus the solution for the time evolution of the magnetic field is given by a linear eigenvalue problem [5, 7, 33, 34]. Correspondingly, to leading order the magnetic energy of the system E^b in the steady state follows an exponential law, more precisely

$$E^b(t) \propto e^{\sigma t}, \quad (7)$$

with σ the fastest growing (or slowest decaying) eigenvalue of the system. In the case $\sigma > 0$, Eq. (7) only holds for a finite range of time, since the hypothesis $E^b \ll E^u$ will be no longer fulfilled as the magnetic energy grows and the decoupling of the induction equation stops being appropriate. The value for which $\sigma = 0$ defines the critical magnetic Reynolds number Rm^{crit} of the dynamo onset, and can be determined numerically by solving the MHD equations for a small enough random magnetic seed and for a large enough exploration of the parameter space [22].

Next we consider the feasibility of attaining self-sustaining convective dynamos employing DNSs of the full non-linear Eqs. (1) to (3). The simulations are performed using the **SPECTER** parallel pseudo-spectral code [26, 27], freely available at [35]. The equations are evolved in time using a double-precision second-order Runge-Kutta method. **SPECTER** represents the fields via Fourier decompositions, attaining spectral convergence for periodic directions, whereas non-periodic ones (\hat{z} in our case) exhibit spectral accuracy inside the domain and very high order convergence at the boundaries. The code employs a standard Fourier decomposition in the periodic directions and a Fourier continuation method with Gram polynomials (FC-Gram) in the non-periodic directions [26, 36], allowing for high-order representation of the boundary conditions without creating Gibbs spectral degradation inside the domain. The absence of magnetic monopoles ($\nabla \cdot \mathbf{b} = 0$) is enforced to machine accuracy by evolving in time the vector potential \mathbf{a} in the Coulomb gauge, defined by $\nabla \times \mathbf{a} = \mathbf{b}$ and $\nabla \cdot \mathbf{a} = 0$. Particularly relevant in the context of this study, **SPECTER** can implement different kinds of electromagnetic boundary conditions while retaining the quasi-spectral convergence properties aforementioned [27] (as a reference, typical errors are $\langle (\nabla \cdot \mathbf{b})^2 \rangle < 10^{-30}$, while quadratic errors in the magnetic boundary conditions are of $\mathcal{O}(10^{-10})$ or smaller). Previous studies of convective dynamos, using other numerical methods or simplified boundary conditions, can be found, e.g., in Refs. [25, 37–40]. For more details of the high-order method used here, or for the full implementation of the electromagnetic boundary conditions, see [27].

III. RESULTS

Role of the boundary conditions at fixed Rayleigh number. We consider first 19 simulations carried over at fixed values of Ra and Re , while varying both the magnetic Reynolds number and the electromagnetic boundary conditions. We will label the simulations using their magnetic Reynolds number, even though their magnetic Prandtl

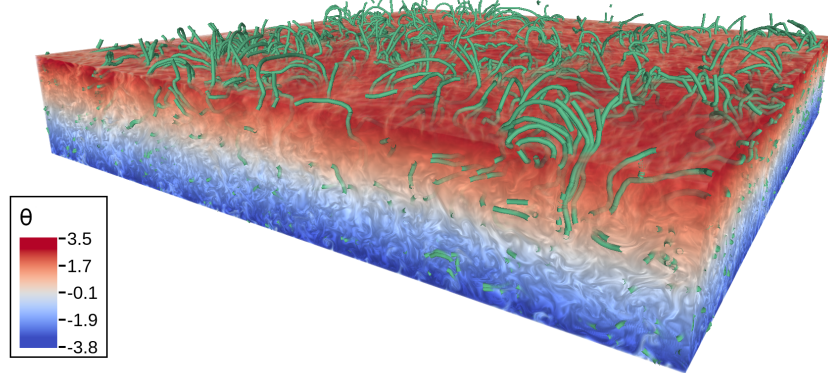


FIG. 1. Rendering using the software VAPOR [41, 42] of the temperature fluctuations θ inside the domain, together with the magnetic field lines (in green) for simulation M22. Note that the magnetic field permeates into the vacuum above $z = 1$.

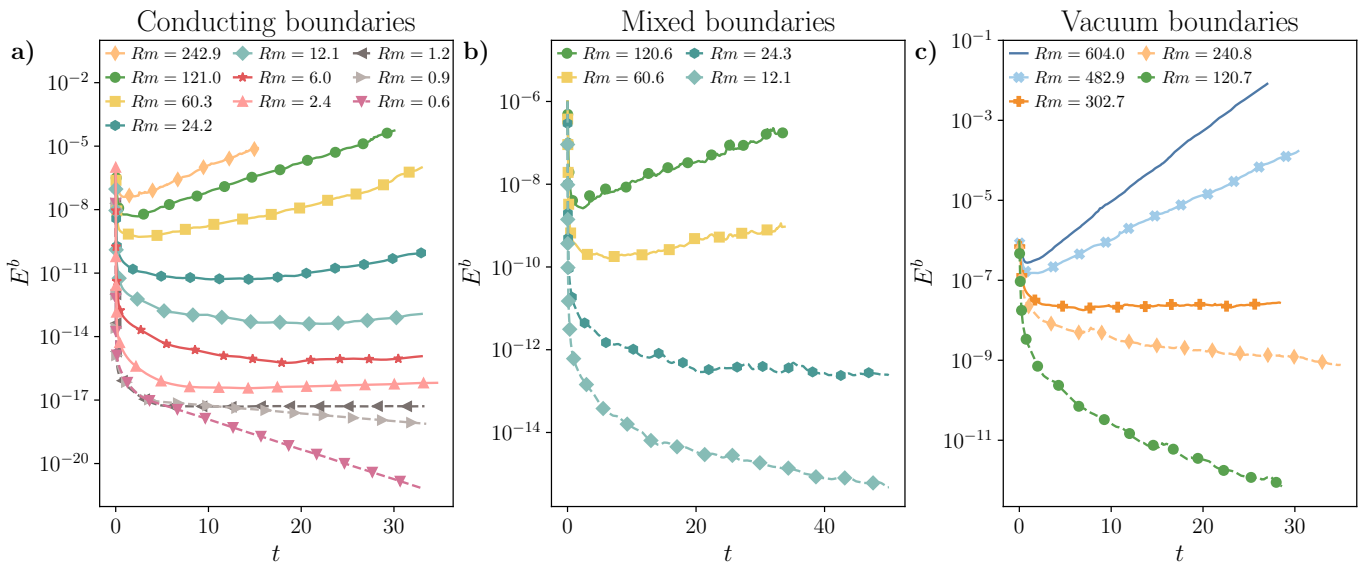


FIG. 2. Magnetic energy E^b as a function of time for all the simulations at $Ra = 2.25 \times 10^6$. Line colors and markers denote the magnetic Reynolds number Rm of each simulation. Panels show a) the case of conducting boundaries, b) mixed boundaries, and c) vacuum surroundings. Simulations with decaying magnetic energy are drawn with discontinuous lines.

number also changes. As we are interested in exploring the regime in which both velocity and temperature fluctuations are dynamically relevant at all scales, the case of $Pr = 1$ is considered. A summary of the runs is presented in Table I. Also, a 3D rendering of both θ and magnetic field lines for a high resolution simulation is shown in Fig. 1.

To carry over the simulations we first integrate the non-magnetic Boussinesq equations (i.e., Eqs. (1) and (3) with $\mathbf{b} = \mathbf{0}$) until a statistically-steady turbulent convective state is attained. The value of Ra is picked so as to have a r.m.s. value of order unity for the flow speed, while keeping the fields well resolved for the chosen spatial resolution. This steady state, together with an initial random magnetic field whose energy is 1×10^{-6} (i.e., six orders of magnitude smaller than that of the temperature and velocity fields), is then used as an initial condition for all the MHD dynamo simulations in Table I. This starting condition is afterwards integrated in time for each of the three electrodynamic scenarios (labeled “C” for conducting boundaries, “M” for mixed boundaries, and “V” for vacuum outside), and values of Rm , until a steady exponential growth or decay in the total magnetic energy is attained.

In Fig. 2 the magnetic energy as a function of time is shown for all the simulations involving each type of boundary

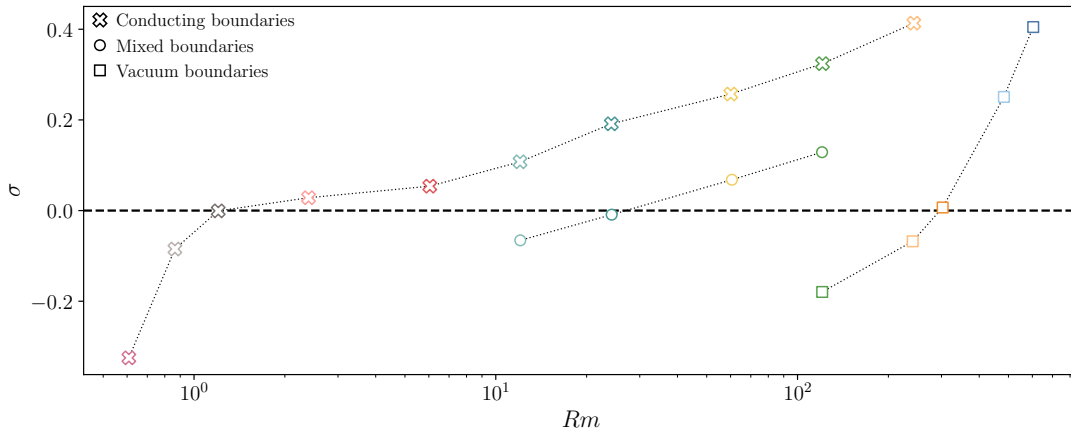


FIG. 3. Growing rate σ as a function of the magnetic Reynolds number Rm for all the simulations at $Ra = 2.25 \times 10^6$. Markers denote the electromagnetic boundary condition used: crosses denote conducting boundaries, circles indicate mixed conditions, and squares designate vacuum surroundings. Dotted lines connect markers of the same type for improved visual clarity.

conditions. The first thing to notice here is that an exponential regime is attained in all the cases (seen as a clear linear trend in the semi-log scale of the figure). This observation is consistent with the fact that a kinematic dynamo regime should be recovered for low amplitude magnetic seeds. Moreover, for all the electromagnetic scenarios under consideration, both growing and decaying steady states are present. However, the most salient point in Fig. 2 is the profound effect of the boundary conditions in the growth rate of the magnetic energy and, by proxy, in the viability of a self-sustaining dynamo process. It can be easily noted that decaying solutions (denoted by discontinuous lines in the figure) are present in the vacuum case at values of Rm much larger than those observed for the cases of mixed boundaries or of two conducting plates. For the latter case, Rm becomes so small in the non-dynamo (decaying) solutions that E^b displays no fluctuations in time, becoming almost insensitive to the flow and purely diffusive.

To characterize the behavior of the growing rate σ as a function of Rm , we perform a least squares fit of the magnetic energy as a function of time in the range for which a steady growth or decay can be observed in each simulation. The results are presented in Fig. 3, where σ is shown as a function of Rm for all the simulations. As noted in Fig. 2, there is a major difference for each type of boundary condition in the value of Rm for which the zero crossings of σ are found. The critical values Rm^{crit} to have the dynamo onset differ by more than an order of magnitude in each case. For conducting plates, a value of $Rm^{\text{crit}} \approx 1.2$ is found, whereas $Rm^{\text{crit}} \approx 30$ for mixed boundary conditions, and $Rm^{\text{crit}} \approx 303$ for vacuum surroundings. It is also interesting to note that for vacuum boundaries σ grows much faster with R_m than in the other cases: once the dynamo is excited (albeit at larger R_m), magnetic energy grows faster.

What dynamo modes are excited in each case? To compare the energy-containing scales of the magnetic solutions, we compute for each simulation the horizontal magnetic spectrum as a function of the horizontal wave number $k_{\parallel} = (k_x^2 + k_y^2)^{1/2}$, $E^b(k_{\parallel}, z)$, in the center of the box $z = L_z/2$, and averaged (after removing the exponential growth or decay) across 10 eddy turnover times. Note *parallel* denotes the directions tangential to the walls. The result is shown in Fig. 4. All the self-sustaining dynamo solutions generate magnetic fields whose energy is concentrated at intermediate and small scales, i.e., the dynamo is a small-scale dynamo. This is compatible with dynamo theory for flows with negligible helicity [1, 9, 43]. Note also in Fig. 4 that as Rm diminishes (i.e., as Ohmic diffusion becomes more relevant at larger scales) the energy containing structures must necessarily shift to lower wave numbers. This fact can be appreciated in the spectra for all three scenarios. Even more, for the case of conducting walls, decaying solutions seem to be obtained only when the diffusive scale is approximately the length of the box, which happens for $Rm \leq 1$. This can also be seen in Fig. 4, where a signature sharp decrease in $E^b(k_{\parallel}, z = L_z/2)$ for $k_{\parallel} = 2$ (i.e., the second smallest wave number) characterizes the solutions incompatible with a self-sustaining dynamo. For the mixed and vacuum boundary conditions cases, however, no such signature feature is found in the spectra for $Rm \approx Rm^{\text{crit}}$.

Another interesting observation is found when comparing the spectra (normalized by the total energy) of the magnetic energy for flows operating at the same Re and Rm values but with differing boundary conditions. This comparison can be found in the inset in Fig. 4c). A clear contrast between the scenarios exhibiting a self-sustained dynamo (i.e., with conducting or mixed boundary conditions) and the magnetic extinction case (vacuum surroundings) is appreciated. The two former present a considerable accumulation of energy at intermediate scales, whereas the latter is dominated by the largest wave numbers of the system.

Role of the Rayleigh number. We now study the dependence of Rm^{crit} on the strength of convection. To this end we pick one scenario for the boundary conditions, namely the mixed case as it is more relevant for the geodynamo,

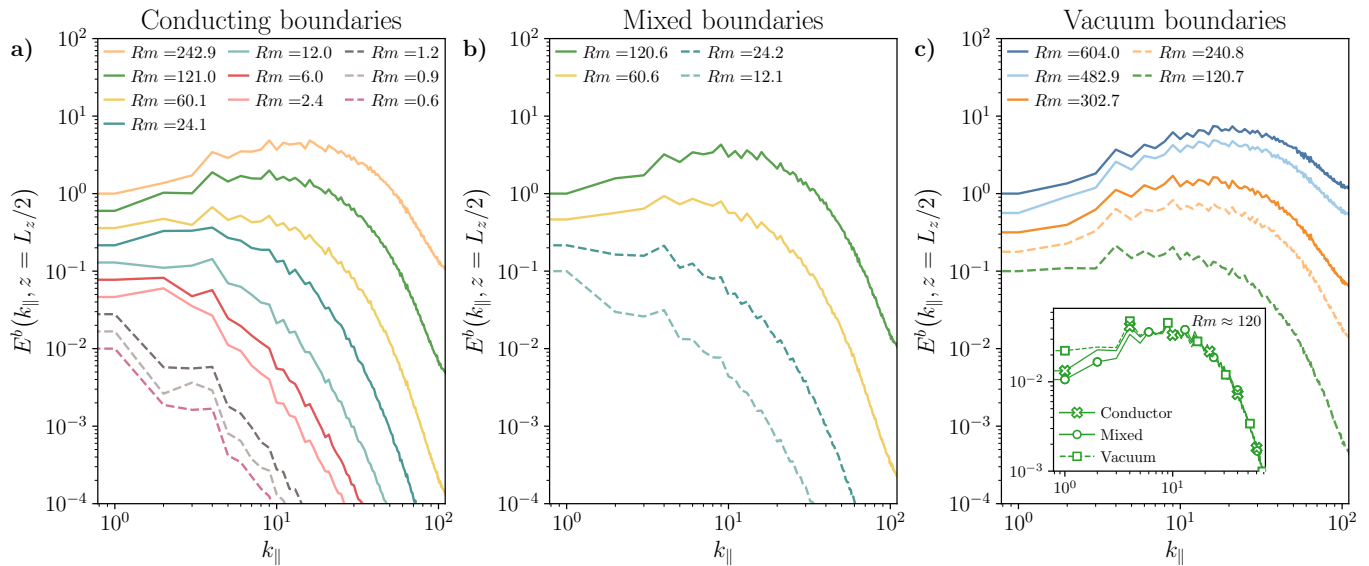


FIG. 4. Magnetic energy spectra $E^b(k_{\parallel}, z)$ for wave numbers in the direction parallel to the wall, k_{\parallel} , at the center of the box ($z = L_z/2$). **a)** Magnetic spectra for runs with conducting boundary conditions. **b)** Same for mixed, and for **c)** vacuum boundaries. In all panels decaying solutions are marked with a discontinuous line, and the colors and symbols reference different values of Rm ($Ra = 2.25 \times 10^6$ in all cases). The inset in panel **c**) shows the normalized spectra for three simulations at the same Rm differing only on their boundary conditions (namely C2, M1 and V5).

TABLE II. Simulations with mixed boundary conditions (i.e., conductor at $z = 0$ and vacuum at $z \geq L_z$). Run lists the label for each simulation. $N_x \times N_y \times N_z$ indicates the spatial resolution, Ra is the Rayleigh number, Re and Rm are the kinetic and magnetic Reynolds number respectively, Pm is the magnetic Prandtl number, and σ is the adjusted growing rate for the magnetic energy, with negative values corresponding to decaying solutions. All simulations have $Pr = 1$.

Run	$N_x \times N_y \times N_z$	Ra	Re	Rm	Pm	σ
M1	$256 \times 256 \times 103$	2.25×10^6	6.03×10^2	1.21×10^2	2.00×10^{-1}	0.12
M2	$256 \times 256 \times 103$	2.25×10^6	6.06×10^2	6.06×10^1	1.00×10^{-1}	0.06
M3	$256 \times 256 \times 103$	2.25×10^6	6.05×10^2	2.42×10^1	4.00×10^{-2}	-0.01
M4	$256 \times 256 \times 103$	2.25×10^6	6.03×10^2	1.21×10^1	2.00×10^{-2}	-0.07
M11	$512 \times 512 \times 231$	9.00×10^6	1.16×10^3	2.91×10^2	2.50×10^{-1}	0.53
M12	$512 \times 512 \times 231$	9.00×10^6	1.15×10^3	1.15×10^2	1.00×10^{-1}	0.01
M13	$512 \times 512 \times 231$	9.00×10^6	1.16×10^3	5.80×10^1	5.00×10^{-2}	-0.02
M14	$512 \times 512 \times 231$	9.00×10^6	1.16×10^3	2.32×10^1	2.00×10^{-2}	-0.13
M21	$1024 \times 1024 \times 487$	3.60×10^7	2.25×10^3	2.81×10^2	1.25×10^{-1}	0.33
M22	$1024 \times 1024 \times 487$	3.60×10^7	2.24×10^3	1.12×10^2	5.00×10^{-2}	0.04
M23	$1024 \times 1024 \times 487$	3.60×10^7	2.25×10^3	5.62×10^1	2.50×10^{-2}	-0.07

and simulate the flow for varying values of Rm , as Ra (and hence, Re) increases. Note that increasing Ra requires a finer grid resolution. In Table II we list the the simulations used for this analysis. For all values of Ra explored, the time evolution of the magnetic energy still presents a short transient after which it reaches an approximately steady growth or decay, in agreement with the kinematic dynamo regime. Figure 5a) shows the dependence of σ as a function of Ra and Rm . For fixed values of Ra , lower values of Rm correspond to lower or negative growth rates. More importantly, it can be readily seen that for a fixed value of Rm , the growth rate becomes smaller as Ra increases. This is particularly relevant, as naturally occurring dynamos usually operate at extreme values of Ra (of order 1×10^{20} or higher [44]). Consequently, a determination of asymptotic values of Rm^{crit} for large Ra would provide better constraints than those found in Fig. 3.

To better analyze this effect we study the behavior of the critical magnetic Reynolds number as a function of Ra . To obtain a representative value for Rm^{crit} from the finite set of simulations available, we pick for each value of Ra the two simulations whose growth/decay rates are closer to zero. We then estimate a linear relation for $\sigma(Rm)$ between said values and obtain Rm^{crit} as the root of that relation. The result is shown in Fig. 5b). Although Rm^{crit} first

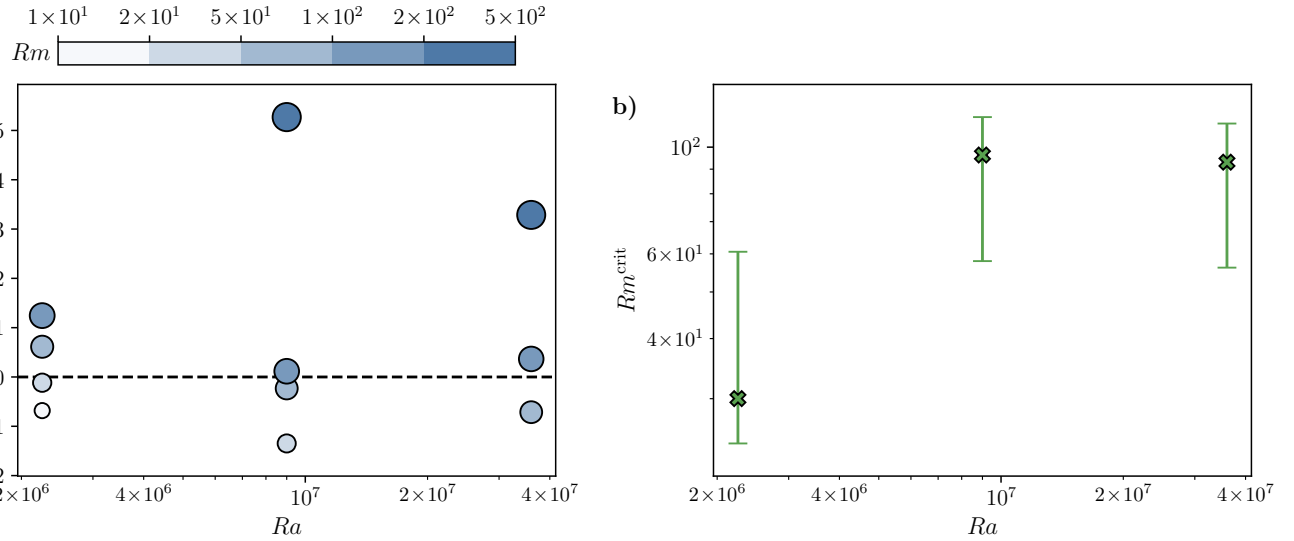


FIG. 5. **a)** Growth rate of the magnetic energy σ as a function of the Rayleigh number Ra , for mixed boundary conditions. Increasing values of the magnetic Reynolds number Rm are denoted both with a darker shade of blue and bigger markers. **b)** Critical magnetic Reynolds number Rm^{crit} as a function of Ra . The horizontal bars denote the Rm values corresponding to the pair of simulations whose growth rates are closer to zero (as shown in panel **a**)), and the crosses correspond to Rm^{crit} obtained as the root of the linear interpolation for $\sigma(Rm)$ between said pair of values.

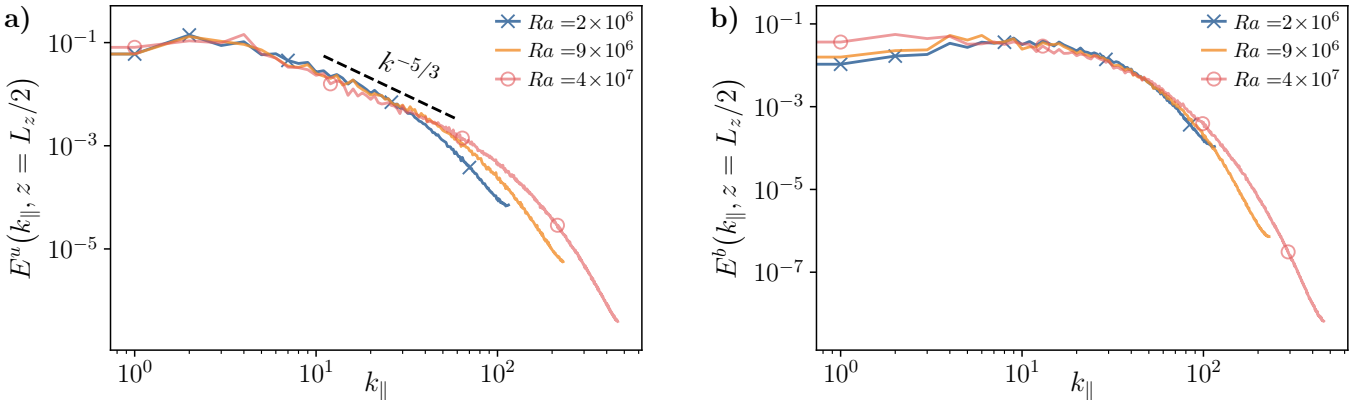


FIG. 6. Energy spectra $E(k_{\parallel}, z)$ as a function of wave numbers parallel to the wall, k_{\parallel} , at the center of the box ($z = L_z/2$) for simulations M4 (blue with crosses), M12 (orange) and M22 (red with empty circles), which operate at approximately the same Rm . **a)** Kinetic energy spectrum E^u , and **b)** magnetic energy spectrum E^b . Spectra are normalized by the total energy.

grows with Ra , it then seems to saturate and remain of $\mathcal{O}(10^2)$ even when Ra is increased fourfold. This could suggest a finite asymptotic value for Rm^{crit} in the limit $Ra \rightarrow \infty$, as suggested in [45] using other methods. Moreover, the order of magnitude obtained is compatible with previous results for this set of boundary conditions [46].

Finally, we consider the effect Ra has on the kinetic and magnetic energy spectra. As before, we use $E(k_{\parallel}, z)$ for that purpose. The resulting spectra, at the center of the box and for runs M4, M12, and M22 (i.e., simulations with different values of Ra but similar Rm) are shown in Fig. 6. In all cases the spectra are well resolved. In Fig. 6a) note that the kinetic energy content at the largest scales is basically indistinguishable among all three simulations. The slope of the spectra for intermediate scales is very similar in all cases, with a power spectrum compatible with a $k^{-5/3}$ power law that extends to larger values of k_{\parallel} as Ra grows. Indeed, it can be readily seen that the kinetic spectra get wider as Ra is increased, as a consequence of a broader inertial range. Contrary to the kinetic energy spectra, the width of the magnetic spectra is observed to remain the same when Ra increases, as shown in Fig. 6b). This is to be expected, as the magnetic Reynolds number is the similar for the three simulations. Conversely, the largest scales of the system seem to be more disparate, containing a greater amount of magnetic energy as Ra increases. This indicates that for larger values of Ra magnetic energy grows at slightly larger scales, albeit at a smaller rate.

IV. DISCUSSION

We studied the problem of attaining a dynamo state in a channel filled with a conducting fluid undergoing turbulent Rayleigh-Bénard convection. To this purpose, we performed multiple direct numerical simulations of the Boussinesq approximation to the MHD equations, utilizing a versatile numerical method with spectral convergence in the bulk of the flow, and very high order convergence near the boundaries [27]. We analyzed the growth or decay of an initially small and random magnetic field as a function of time, determining the critical magnetic Reynolds number Rm^{crit} for which self-sustaining dynamo action becomes feasible for three electromagnetic boundary conditions at the floor and the top of the channel at fixed Ra , and then by varying Ra for a fixed boundary condition.

The effect of changing boundary conditions is particularly relevant for dynamo experiments, as previous laboratory experiments have shown a strong sensitivity of the dynamo onset to the electromagnetic properties of the containing vessel and of the propellers. For the convective case, we analyzed dynamo feasibility for three sets of boundary conditions: both plates perfectly conducting, both walls surrounded by vacuum (with a potential magnetic field outside the domain), and a combination of a conducting floor with vacuum outside the top of the channel. In all the cases the magnetic energy was observed to grow or decrease exponentially in time, allowing for the determination of growth or decay rates, and of critical values for dynamo action. Sharp differences, of one order of magnitude or more, were observed in Rm^{crit} for each set of boundary conditions, with the fully conducting case showing the mildest constraint and the entirely vacuum scenario displaying the most severe restriction. Therefore, and consistently with experiments, utilizing conducting materials seems to be notably advantageous for achieving self-sustaining dynamos.

Raising the strength of convection and turbulence results in a growth of Rm^{crit} , as also observed in previous studies using fully periodic setups. Nevertheless, the observed effect seems to asymptote to values of Rm^{crit} independent of Ra . In all cases, dynamos generate magnetic fields at intermediate scales, with magnetic energy spectra that peak at scales smaller than the flow integral scale.

ACKNOWLEDGMENTS

The authors acknowledge support from CONICET and ANPCyT through PIP, Argentina Grant No. 11220150100324CO, and PICT, Argentina Grant No. 2018-4298. We also thank the Physics Department at the University of Buenos Aires for providing computing time on its Dirac cluster.

-
- [1] A. Pouquet, U. Frisch, and J. Léorat, Strong mhd helical turbulence and the nonlinear dynamo effect, *Journal of Fluid Mechanics* **77**, 321– (1976).
- [2] A. Brandenburg and K. Subramanian, Astrophysical magnetic fields and nonlinear dynamo theory, *Physics Reports* **417**, 1 (2005).
- [3] G. Verhille, N. Plihon, M. Bourgoin, P. Odier, and J.-F. Pinton, Laboratory Dynamo Experiments, *Space Science Reviews* **152**, 543 (2010).
- [4] S. Tobias, The turbulent dynamo, *Journal of Fluid Mechanics* **912**, P1 (2021).
- [5] P. M. Mannix, Y. Ponty, and F. Marcotte, Systematic route to subcritical dynamo branches, *Phys. Rev. Lett.* **129**, 024502 (2022).
- [6] C. A. Jones, 8.05 - thermal and compositional convection in the outer core, in *Treatise on Geophysics*, edited by G. Schubert (Elsevier, Amsterdam, 2007) pp. 131–185.
- [7] P. H. Roberts and E. M. King, On the genesis of the Earth’s magnetism, *Reports on Progress in Physics* **096801**, 10.1088/0034-4885/76/9/096801 (2013).
- [8] T. G. Cowling, The Magnetic Field of Sunspots, *Monthly Notices of the Royal Astronomical Society* **94**, 39 (1933).
- [9] F. Krause and K. H. Radler, *Mean-Field Magnetohydrodynamics and Dynamo Theory* (Pergamon Press, 1980).
- [10] A. Gailitis, O. Lielausis, S. Dement’ev, E. Platacis, A. Cifersons, G. Gerbeth, T. Gundrum, F. Stefani, M. Christen, H. Hänel, and G. Will, Detection of a Flow Induced Magnetic Field Eigenmode in the Riga Dynamo Facility, *Physical Review Letters* **84**, 4365 (2000).
- [11] U. Müller and R. Stieglitz, The Karlsruhe Dynamo Experiment, *Nonlinear Processes in Geophysics* **9**, 165 (2002).
- [12] M. D. Nornberg, E. J. Spence, R. D. Kendrick, C. M. Jacobson, and C. B. Forest, Intermittent magnetic field excitation by a turbulent flow of liquid sodium, *Physical Review Letters* **97**, 74 (2006).
- [13] N. Schaeffer, D. Jault, H.-C. Nataf, and A. Fournier, Turbulent geodynamo simulations: a leap towards Earth’s core, *Geophysical Journal International* **211**, 1 (2017).
- [14] M. Fontana, P. D. Mininni, and P. Dmitruk, Magnetic structure, dipole reversals, and 1/f noise in resistive MHD spherical dynamos, *Physical Review Fluids* **3**, 1 (2018).

- [15] G. Glatzmaier and P. Roberts, A three-dimensional self-consistent computer simulation of a geomagnetic field reversal, *Nature* **377**, 203 (1995).
- [16] R. Monchaux, M. Berhanu, S. Aumaître, A. Chiffaudel, F. Daviaud, B. Dubrulle, F. Ravelet, S. Fauve, N. Mordant, F. Pétrélis, M. Bourgoin, P. Odier, J. Pinton, N. Plion, and R. Volk, The von Kármán Sodium experiment: Turbulent dynamical dynamos, *Physics of Fluids* **21**, 35108 (2009).
- [17] M. Berhanu, G. Verhille, J. Boisson, B. Gallet, C. Gissinger, S. Fauve, N. Mordant, F. Pétrélis, M. Bourgoin, P. Odier, J. F. Pinton, N. Plion, S. Aumaître, A. Chiffaudel, F. Daviaud, B. Dubrulle, and C. Pirat, Dynamo regimes and transitions in the VKS experiment, *European Physical Journal B* **77**, 459 (2010).
- [18] P. Olson, Experimental Dynamos and the Dynamics of Planetary Cores, *Annual Review of Earth and Planetary Sciences* **41**, 153 (2013).
- [19] C. M. Cooper, J. Wallace, M. Brookhart, M. Clark, C. Collins, W. X. Ding, K. Flanagan, I. Khalzov, Y. Li, J. Milhone, M. Nornberg, P. Nonn, D. Weisberg, D. G. Whyte, E. Zweibel, and C. B. Forest, The Madison plasma dynamo experiment: A facility for studying laboratory plasma astrophysics, *Physics of Plasmas* **21**, 10.1063/1.4861609 (2014).
- [20] D. S. Zimmerman, S. A. Triana, H. C. Nataf, and D. P. Lathrop, A turbulent, high magnetic reynolds number experimental model of earth's core, *Journal of Geophysical Research: Solid Earth* **119**, 4538 (2014).
- [21] R. E. Rojas, A. Perevalov, T. Zürner, and D. P. Lathrop, Experimental study of rough spherical couette flows: Increasing helicity toward a dynamo state, *Phys. Rev. Fluids* **6**, 033801 (2021).
- [22] Y. Ponty, P. D. Mininni, D. C. Montgomery, J. F. Pinton, H. Politano, and A. Pouquet, Numerical study of dynamo action at low magnetic Prandtl numbers, *Physical Review Letters* **94**, 1 (2005).
- [23] A. Jackson, A. Sheyko, P. Marti, A. Tilgner, D. Cébron, S. Vantieghem, R. Simitev, F. Busse, X. Zhan, G. Schubert, S. Takehiro, Y. Sasaki, Y.-Y. Hayashi, A. Ribeiro, C. Nore, and J.-L. Guermond, A spherical shell numerical dynamo benchmark with pseudo-vacuum magnetic boundary conditions, *Geophysical Journal International* **196**, 712 (2013).
- [24] M. Sadek, A. Alexakis, and S. Fauve, Optimal length scale for a turbulent dynamo, *Phys. Rev. Lett.* **116**, 074501 (2016).
- [25] J. Varela, S. Brun, B. Dubrulle, and C. Nore, Effects of turbulence, resistivity and boundary conditions on helicoidal flow collimation: Consequences for the Von-Kármán-Sodium dynamo experiment, *Physics of Plasmas* **24**, 10.1063/1.4983313 (2017).
- [26] M. Fontana, O. Bruno, P. Mininni, and P. Dmitruk, Fourier continuation method for incompressible fluids with boundaries, *Computer Physics Communications* **256**, 10.1016/j.cpc.2020.107482 (2020).
- [27] M. Fontana, P. D. Mininni, O. P. Bruno, and P. Dmitruk, Vector potential-based MHD solver for non-periodic flows using Fourier continuation expansions, *Computer Physics Communications* **275**, 108304 (2022).
- [28] M. Meneguzzi and A. Pouquet, Turbulent dynamos driven by convection, *Journal of Fluid Mechanics* **205**, 297 (1989).
- [29] C. A. Jones and P. H. Roberts, Convection-driven dynamos in a rotating plane layer, *Journal of Fluid Mechanics* **404**, 311 (2000).
- [30] A. Gailitis, O. Lielausis, E. Platacis, G. Gerbeth, and F. Stefani, Colloquium: Laboratory experiments on hydromagnetic dynamos, *Reviews of Modern Physics* **74**, 973 (2002).
- [31] J. Wicht, Inner-core conductivity in numerical dynamo simulations, *Physics of the Earth and Planetary Interiors* **132**, 281 (2002).
- [32] J. D. Jackson, *Classical Electrodynamics*, 2nd ed. (Wiley, 1975).
- [33] K. Moffatt, *Magnetic Field Generation in Electrically Conducting Fluids* (Cambridge University Press, 1978).
- [34] P. Roberts and G. Glatzmaier, Geodynamo theory and simulations, *Reviews of Modern Physics* **72**, 1081 (2000).
- [35] M. Fontana and P. D. Mininni, SPECTER (Special PEriodic Continuation Turbulence solvER), <https://github.com/mfontanaar/SPECTER>.
- [36] O. P. Bruno and M. Lyon, High-order unconditionally stable FC-AD solvers for general smooth domains I. Basic elements, *Journal of Computational Physics* **229**, 2009 (2010).
- [37] J.-C. Thelen and F. Cattaneo, Dynamo action driven by convection: the influence of magnetic boundary conditions, *Monthly Notices of the Royal Astronomical Society* **315**, L13 (2000).
- [38] F. Cattaneo, T. Emonet, and N. Weiss, On the interaction between convection and magnetic fields, *The Astrophysical Journal* **588**, 1183 (2003).
- [39] L. Chen, W. Herreman, and A. Jackson, Optimal dynamo action by steady flows confined to a cube, *Journal of Fluid Mechanics* **783**, 23 (2015).
- [40] M. R. Proctor, Energy requirement for a working dynamo, *Geophysical and Astrophysical Fluid Dynamics* **109**, 611 (2015).
- [41] J. Clyne, P. Mininni, A. Norton, and M. Rast, Interactive desktop analysis of high resolution simulations: application to turbulent plume dynamics and current sheet formation, *New Journal of Physics* **9**, 301 (2007).
- [42] S. Li, S. Jaroszynski, S. Pearse, L. Orf, and J. Clyne, Vapor: A visualization package tailored to analyze simulation data in earth system science, *Atmosphere* **10**, 10.3390/atmos10090488 (2019).
- [43] A. A. Schekochihin, S. Cowley, S. Taylor, G. Hammett, J. Maron, and J. McWilliams, Saturated state of the nonlinear small-scale dynamo, *Physical Review Letters* **92**, 084504 (2004).
- [44] P. Olson, 8.01 - overview, in *Treatise on Geophysics*, edited by G. Schubert (Elsevier, Amsterdam, 2007) pp. 1–30.
- [45] J. Léorat, A. Pouquet, and U. Frisch, Fully developed mhd turbulence near critical magnetic reynolds number, *Journal of Fluid Mechanics* **104**, 419–443 (1981).
- [46] P. Bushby, B. Favier, M. Proctor, and N. Weiss, Convectively driven dynamo action in the quiet sun, *Geophysical & Astrophysical Fluid Dynamics* **106**, 508 (2012).